Macromolecules

ARTICLE

pubs.acs.org/Macromolecules

Multiscale Simulation Study on the Curing Reaction and the Network Structure in a Typical Epoxy System

Hong Liu,[†] Min Li,[*,‡] Zhong-Yuan Lu,[*,†] Zuo-Guang Zhang,[‡] Chia-Chung Sun,[†] and Tian Cui[§]

[†]Institute of Theoretical Chemistry, State Key Laboratory of Theoretical and Computational Chemistry, Jilin University, Changchun 130023, China

[‡]Key Laboratory of Aerospace Materials and Performance (Ministry of Education), School of Materials Science and Engineering, Beihang University, Beijing 100083, China

[§]National Laboratory of Superhard Materials, Jilin University, Changchun 130012, China

ABSTRACT: We propose a multiscale simulation strategy to study the interplay between diffusion and curing reaction on the network formation and the corresponding mechanical properties of epoxy resins. Atomistic molecular dynamics simulations are first used to estimate the parameters that will be used in coarse-grained simulations. Then a dissipative particle dynamics coupled with curing reaction model is developed and adopted to simulate the cross-linking process of the system to form an epoxy network structure. We find that, during the curing process, to which extent that the components can diffuse between each other greatly influences the generated network structure. Finally, the reverse mapping of the coarse-grained structure to atomistic representation is carried out to analyze the mechanical properties and the T_g of the epoxy resin system.

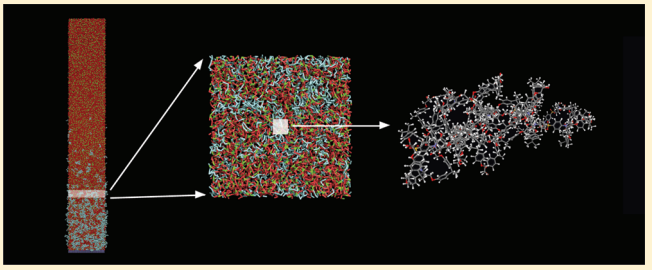

1. INTRODUCTION

Monomers bearing multifunctional groups may form highly cross-linked network structures due to, e.g., polycondensation. For example, in common epoxy molecules, there are two or more epoxy groups which can react with the active hydrogens in amines of the curing agents.[1] The products with cross-linked network structures exhibit excellent thermal stability, high static modulus, low creep, and high-temperature performance, etc. As a result, these materials are widely applied as electronic packaging, bonding agents, and in aerospace industry as coatings, composites, and adhesives. In practice, what is the network formation mechanism at microscale and how to control the network structure are the main concerns in the applications. To elucidate these concerns, a lot of theoretical, experimental, and computational studies had emerged in recent years.[1−20]

Theoretical studies on the formation of polymeric network structures can be traced back to 1940s. The pioneer works by Flory[21] and Stockmayer[22] built up the theoretical protocols to deal with the network formation of monomers with multifunctional groups. Subsequently, other theoretical models and treatments on the curing reactions were successfully developed; they presented a general view on the polymeric network formation process and the resulted statistical properties.[6−8,23,24] However, these statistical curing theories can not supply much information about the microscopic network structures and the properties such as solvent adsorption and inhomogeneous swelling, which are of particular interest in applications. In experiments, the atomistic distributions in polymer network structures can be measured by small angle neutron scattering or other relevant apparatus.[25] But the local network information, such as the number of cross-links between monomers, the accurate cross-linking density and distributions, can not be readily obtained in experiments.

As a feasible route to validating experimental results and predicting new phenomena, computer simulation becomes especially important on presenting microscopic network structures and the corresponding physical properties.[26] Coarse-grained (CG) simulation models for polymer networks were developed since 1990s, and the results improved our understanding on polymer network formation and properties.[27−36] However, these CG models can not supply enough atomistic information to specific polymer network systems such as epoxy resin. Therefore, a direct comparison between specific experimental and CG simulation results is very difficult. Recently, atomistic molecular dynamics (MD) simulation method was mostly chosen in the literatures to describe the network formation of specific polymer systems, since the method can reflect the local network structures with atomistic details and manifest the relation between the mechanical properties of the materials and the resin network structures. For example, Yarovsky and Evans proposed a method to predict cross-linking density in the mixture of epoxy and curing agent molecules, and further investigated the adhesion strength between the cured epoxy resin and an inorganic substrate.[9] Gou et al. used MD simulations to construct the

Received: June 20, 2011
Revised: September 2, 2011
Published: October 17, 2011

cross-linked networks for epoxy resins to predict the interfacial shear strength.[10] Wu and Xu also used a cross-linking procedure based on MD simulations to build the epoxy resin networks and studied the diffusion of water in the cross-linked structures.[11] Komarov et al. proposed a multiscale simulation scheme to generate highly cross-linked epoxy resins and studied the dependence of glass transition temperature on the functional group conversion.[26] Höstermann et al. combined MD simulations with Kamal equation to define the chemical reaction kinetic constants of epoxy systems which can reflect the curing process, and studied water adsorption and network swelling.[37]

In general, two typical ways were employed for building cross-linked network structures in previous studies.[13] The first way is "reacting" the mixture of monomers and cross-linking agents by manually connecting the adjacent functional groups in the simulations. For example in ref 9, all the possible cross-linking reactions were manually carried out simultaneously by checking an artificial reaction radius. The other way is using the coarse-grained model to build a cross-linked network structure and further map it back to the atomistic model. This strategy was adopted by Komarov et al.,[26] who designed a continuous procedure using Monte Carlo (MC) and MD hybrid method to study the relation between the functional group conversions and the mechanical properties of epoxy resins. The multiscale simulation procedure includes mapping the atomistic model to a CG model, generating the cross-linked network based on the CG model via MC method, reverse mapping the CG model to fully atomistic representation, and finally simulating the model with standard MD technique. The advantage of multiscale simulation methods resides in the fact that, larger length and time scales, which are prerequisite to correctly describe a realistic network structure, can be accessed with much reduced computational resources.

Here we propose a multiscale simulation strategy to reasonably generate chemical network structures by incorporating both particle diffusion and curing reactions in coarse-grained models. The current work builds upon our experiences on multiscale simulation[38,39] and particle based simulation coupled with chemical reactions,[40−42] and is enlightened by the work of Komarov et al.[26] There are also four steps in our multiscale simulation strategy, i.e.: (1) building up coarse-grained model from an atomistic system; (2) generating network structures with the coarse-grained model by using hybrid dissipative particle dynamics and Monte Carlo methods; (3) reverse-mapping atomistic network structures from the coarse-grained model; and (4) computing thermodynamic, dynamic and mechanical properties of the specific network structures. This multiscale simulation strategy shares the same advantage with the work of Komarov et al., but the main difference is that the competition between component diffusion and chemical reaction is inherently incorporated in our model, so complex systems characterized by inhomogeneous network structures can be easily generated and studied.

We then use this model to solve a typical problem in polymer composite industry, i.e., the formation of epoxy resin with carbon fibers. Normally, commercial carbon fibers are covered by a layer of sizing agent, in most cases composed by epoxy molecules with high molecular weight. The existence of the sizing agent introduces new interfaces between epoxy resin and carbon fibers, consequently influences the properties of the produced composites. Thus, the mechanism of the epoxy network formation and the corresponding network structure with the existence of sizing agent are the most important issues to be clarified for manufacturing satisfactory composites. However in experiments, it is not easy to *in situ* measure the variation of the network structures during the curing process. Simultaneously incorporating dynamic interface and network formation is also difficult for earlier simulation models. Our proposed multiscale simulation strategy is suitable to deal with this problem. We thus construct the coarse-grained dissipative particle dynamics (DPD) model coupled with curing reaction to simulate the formation of cross-linked network structures for the complex system composed of carbon fiber, sizing agent, and epoxy molecules. We further investigate the gradient distributions of the components and the cross-linking points along the direction perpendicular to the carbon fiber surface, and the mechanical properties of local network structures in the composite. It should be noted that our multiscale simulation strategy is not limited to this specific system only. Actually, it can be further adopted in more complex systems in which different competing dynamic factors take effects simultaneously.

The paper is organized as follows: section 2 exhibits the multiscale modeling strategy and simulation details, section 3 shows the results and the corresponding discussion, and finally, section 4 presents the concluding remarks.

2. MODEL AND SIMULATION DETAILS

We will show how the multiscale simulation strategy is carried out by focusing on an experimentally important system. In general, the commercial carbon fibers will be coated by a layer of sizing agent with several tens of nanometer in thickness. Therefore, the properties of the composite formed by carbon fibers and epoxy molecules are strongly dependent on the interfaces between sizing agent and epoxy molecules, the diffusion of curing agent from epoxy phase to sizing agent phase, and the network structures and the cross-link distributions along the direction perpendicular to the carbon fiber surface. To elucidate these influences, a model system containing the inorganic carbon fiber surface, a layer of sizing agent with several tens of nanometer in thickness, and a thick layer of epoxy molecules mixed with curing agents is needed.

The epoxy molecule diglycidyl ether of bisphenol A (DGEBA), which will be denoted by RA in the following, and the curing agent 4,4′-diaminodiphenyl sulfone (DDS), are considered here to form the epoxy phase. The molar mass for RA with $n = 1$, as shown in Figure 1a, is $M_{RA} = 624.8$ g/mol. The sizing agent (denoted by SA in the following) is also a kind of epoxy molecule but with a larger number of repeat unit. The experimental mean molar mass of SA $M_{SA} = 2900$ g/mol defines the number of repeat unit $n = 9$ in this study, as shown in Figure 1a.

Three principal reactions can take place in the epoxy system,[1] as shown in Figure 1c. During the curing reactions, the epoxy group first reacts with one primary amine of the curing agent (in the following we note this step of reaction as "primary curing" reaction). The resulted secondary amine can further react with other epoxy molecules and form a ternary amine (in the following this step of the reaction is noted as a "secondary curing" reaction). Moreover, the newly generated hydroxyl group from the opened epoxy group can further react with another epoxy to form an ether linkage. As the reaction continues, a complex polymer network structure will be generated.

We then consider to build up a simulation model with unmovable surface particles representing carbon fiber surface, a

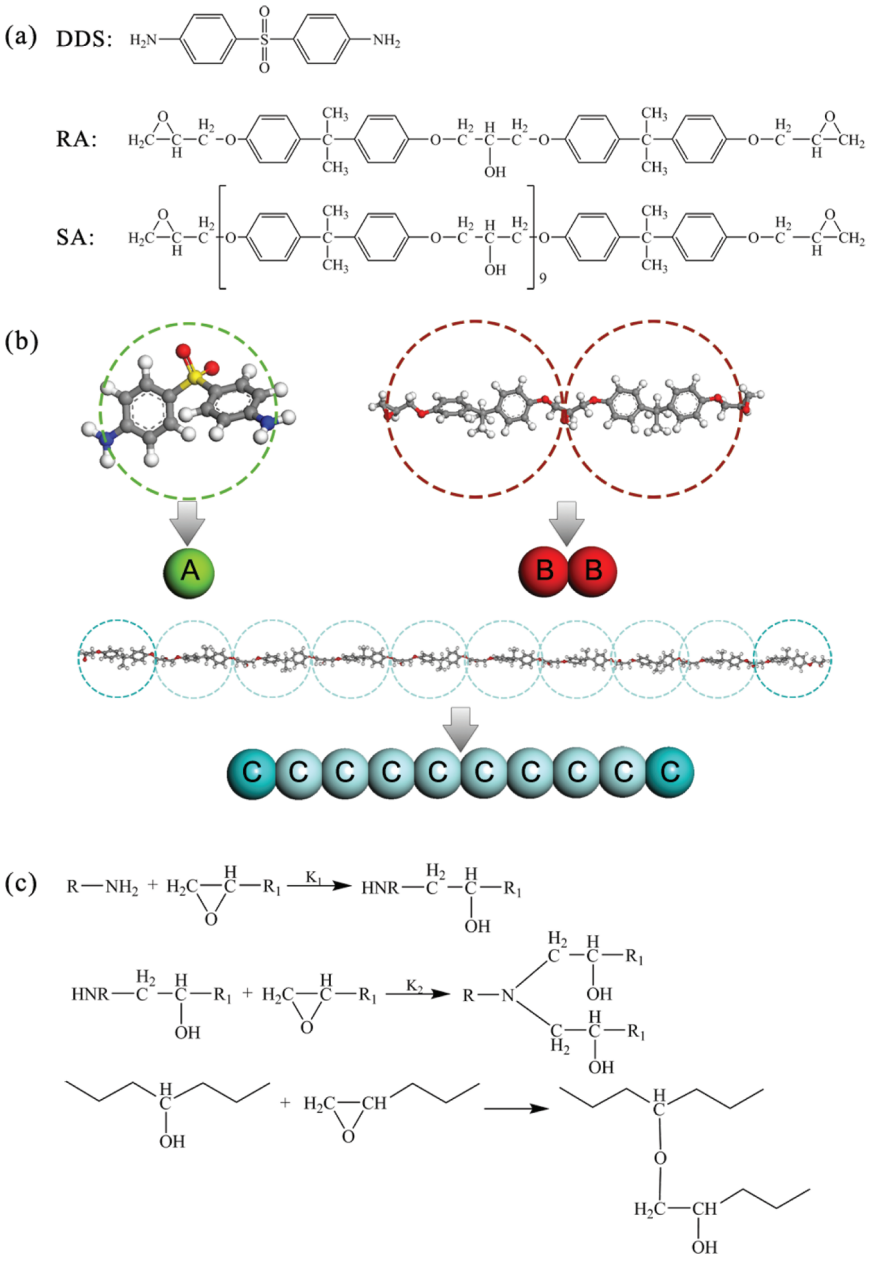

Figure 1. (a) Molecular formula of DDS, RA, and SA; (b) schematic illustration of the coarse-graining scheme for the three components; (c) three principal reactions in the epoxy system.

layer of sizing agent on top of this surface, and another layer of epoxy molecules mixed with DDS. In the simulation model, the z axis is chosen to be perpendicular to the carbon fiber surface. To reasonably reflect the diffusion process and the network structures, this model system should be large enough. Since the experimental SA layer is several tens of nm in thickness, we consider that the minimum layer thickness should be larger than 20 nm. Therefore, we may need to construct a, for example, 25 × 25 × 25 nm^3 model SA system on top of the unmovable inorganic surface to represent this layer in our simulations. Practically, the RA layer is at least several times thicker than the SA layer. Thus, we may assume that RA layer is 5 times thicker than SA, so a 25 × 25 × 125 nm^3 model RA system on top of the SA layer should be constructed further. Therefore, about 10 million atoms will be included in this complex system. Such a system is far too large for atomistic MD simulations, thus the multiscale simulation strategy is inevitable needed to solve this problem.

Similar to the work of Komarov et al.,[26] our multiscale simulation strategy includes the following four steps: (a) design the mapping scheme between the atomistic structures and the coarse-grained DPD beads and define the parameters in DPD simulations; (b) do the mesoscale simulations by DPD coupled with reactions to model the process of diffusion and the curing reactions; (c) choose representative local network structures and reverse-map them onto the atomistic structures; (d) apply the standard MD simulations to analyze the properties of the network structures.

2.1. The Coarse-Graining Scheme. Figure 2 shows the schematic system to be simulated. In DDS/RA layer, the molar

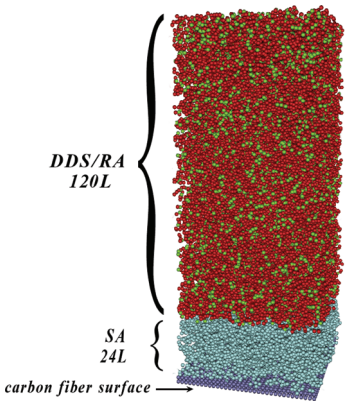

Figure 2. Schematic illustration of the initial layered structure of the epoxy/DDS and the sizing agent. Note that, L = 1.07 nm in this study.

ratio between DDS and RA is 1:2, so that the functional group ratio between reactive hydrogen atoms in primary amines and epoxy groups is 1:1, i.e., the epoxy groups can consume all reactive hydrogen atoms to form the ternary amines in DDS if the curing reaction is thoroughly accomplished. If the thickness ratio between RA/DDS and SA is 5, the volume fractions of the components are therefore: ϕ_{DDS} = 0.28, ϕ_{RA} = 0.56, and ϕ_{SA} = 0.16.

According to the structural characteristics of the three kinds of molecules, we propose the following coarse-graining scheme: the curing agent DDS is represented by one CG bead, the RA is coarse-grained into two CG beads, and the SA with repeat unit number n = 9 is represented by a 10-bead chain. We define n_b as the CG bead number of each component, thus $n_{b_{DDS}} = 1$, $n_{b_{RA}} = 2$, and $n_{b_{SA}} = 10$. As a result, as illustrated in Figure 1b, there are three types of beads, A, B, and C in our coarse-grained model, in which A denotes DDS, B denotes RA, and C denotes SA. Some of the beads are taken as reactive ones which contain the amine or epoxy groups, such as the DDS beads and the terminal beads in RA or SA chains (indicated by the highlighted beads in Figure 1b). Subsequently, we need to estimate their average density, molar mass, and volume, as requested by the coarse-grained DPD simulations.

As shown in experiments,[43] 150 °C (423 K) is the most important temperature of curing process for the epoxy/carbon fiber composite system. Therefore, in our simulations, we exclusively focus on this temperature and try to show molecular details of the curing process in the epoxy/carbon fiber composites. First of all, we run atomistic MD simulations in the *NPT* ensemble to estimate the densities of pure components at experimental temperature (423 K). The initial configurations are constructed via amorphous cell tool in Materials Studio[44] followed by structural relaxations. The simulation box side lengthes are at least 22 Å, depending on the types of the components and the corresponding experimental densities. Here we choose COMPASS force field since it has been well validated.[45] Then the atomistic MD simulations are carried out in NPT ensemble at T = 423 K. The Berendsen thermostat and barostat are adopted in the simulations.[46] The time step is chosen as 1.0 fs, and the MD simulations are conducted for 500 ps. The van der Waals interactions are based on a cutoff treatment at 10.0 Å and the Coulomb interactions are dealt with standard Ewald summation.[47] During the simulations, we trace the time evolution of system density to judge the equilibrium. When the system

Table 1. Molar Mass and the Volume Fraction of the Three Types of CG Beads

bead type	A	B	C
M (g/mol)	248.30	312.40	289.97
ϕ	0.66	0.17	0.17

density approaches to a plateau value and fluctuates with almost the same amplitude below and above the average density, we will take the part of trajectory starting from this time as the equilibrium states. In practice, five independent parallel simulations are carried out to verify the equilibrium and to make sure that the data are collected in equilibrium states. From the equilibrium data in the MD simulations, we can estimate the component densities at 423 K: ρ_{DDS} = 1.17 g/cm^3 and $\rho_{RA} = \rho_{SA}$ = 1.04 g/cm^3. Thus, the average density of the system is $\overline{\rho} = \phi_{DDS} \times \rho_{DDS} + \phi_{RA} \times \rho_{RA} + \rho_{SA}$ = 1.08 g/cm^3.

As suggested in ref 48, a basic assumption in DPD method is that all CG beads possess comparable masses and volumes. It is easy to obtain the molar masses of each types of CG beads from their respective underlying molecular formula, as shown in Table 1. The volume fractions of each types of CG components are also given in Table 1. Although the masses of the beads are different, we assume that we still can use the mean molar mass of the beads to define a single mass unit: $m = \Sigma_{i=A\sim C}(\phi_i \times M_i)$ = 266.28 g/mol. From this mean molar mass and the average density, we can obtain the average volume of the CG bead as $\overline{v}$ = 409.42 Å^3. We then use the average mass and volume to define the mass and length units in our CG simulations. In classical CG DPD simulations, the reduced bead number density is chosen as ρ_n = 3. Thus, following the handling of DPD simulations in ref 48, we can define the length scale of the simulation as $L = (\overline{v}\rho_n)^{1/3}$ = 1.07 nm. This length scale denotes that there are 3 CG DPD beads in a small cell of size L^3. As conventionally used in DPD simulations, the interaction radius of CG beads, r_c, is set equal to L.

In this study, we mainly focus on the interplay of the component diffusion and the curing reaction on the physical properties of the network structure, thus the model of carbon fiber is reduced to a simple surface and any possible bonded interactions between the components and the carbon fiber surface (such as the experimentally possible curing reaction between amine groups in DDS and dangling epoxy groups on carbon fiber surface) are omitted. In the corresponding experiments, the carbon fiber with a diameter of about 6−7 μm was adopted.[43] In our simulations, we only consider a small patch of carbon fiber surface with side length about 26 nm. Thus, as compared with typical carbon fiber diameter, the small patch of carbon fiber surface adopted here can be approximately taken as a planar wall. Two layers of regularly arranged and densely packed frozen DPD beads are utilized to construct the wall (the periodic boundary conditions are applied in both x and y directions but not in z direction which is the normal direction of the surface).[42] The distance between the two layers of beads in the wall, d_L, is determined by the density of the wall beads ρ_W, i.e., $d_L = {\rho_W}^{-1/3}$. In this study, we choose ρ_W = 3 to avoid the perturbation of density distribution in bulk phase that may be induced by the density difference between the solid wall and the bulk phase, thus d_L = 0.69. The wall is neutral, namely, there is no incompatibility between the component beads (including RA, SA, and DDS beads) and the wall beads.[42,49] Furthermore, to keep the wall impenetrable, when a component bead hits the wall due to the

integration of equations of motion, a bounce-back reflection condition is imposed so that the bead can move back into the bulk phase.[50]

For easy numerical handling, we construct the simulation box of size $24 \times 24 \times 144\, L^3$ with reduced bead number density $\rho_n = 3$; consequently, our CG DPD model consists of 248832 movable beads. In the beginning of the CG simulations, this box is divided into two parts along the z direction: the lower region with thickness of $24L$ is considered as the SA layer, thus all of the SA chains are randomly generated in this region; the upper part with height of $120L$ is the DDS/RA layer, thus the DDS beads and the RA short chains are randomly generated with molar ratio 1:2 in this region. After the generation of the initial configuration, there is an apparent interface between the two layers. The simulations with mutual diffusion and the curing reactions will start from this configuration, as schematically illustrated in Figure 2.

2.2. DPD Method and Lowe−Andersen Thermostat. In DPD method, the time evolution of the interacting CG beads is governed by Newton's equations of motion.[51] Interbead interactions are characterized by pairwise conservative, dissipative, and random forces acting on a bead i by a bead j. The conservative force takes the form $\mathbf{F}_{ij}^C = -\alpha_{ij}\omega^C(r_{ij})\mathbf{e}_{ij}$, and the dissipative and random forces couple together to form an effective thermostat. $\mathbf{e}_{ij} = \mathbf{r}_{ij}/r_{ij}$ with $\mathbf{r}_{ij} = \mathbf{r}_i - \mathbf{r}_j$ and $r_{ij} = |\mathbf{r}_{ij}|$, and α_{ij} is the repulsion strength, which takes the value of 25 for the beads of same kind in our simulations.[51] The parameter α_{ij} between differing species is often set larger than 25, representing the degree of incompatibility between them. $\omega^C(r_{ij}) = 1 - r_{ij}/r_c$ for $r_{ij} < r_c$ and $\omega^C(r_{ij}) = 0$ for $r_{ij} \geq r_c$ such that the conservative forces are soft and repulsive.

The radius of interaction, the bead mass, and the temperature are set as the units in our DPD simulations, i.e. $r_c(= L) = m = k_BT \equiv 1$. Polymers are constructed by connecting the neighboring beads together via the harmonic springs $\mathbf{F}_i^S = \Sigma_j C\mathbf{r}_{ij}$. We choose the spring constant $C = 10$ according to ref 52. The time step is set as $\Delta t = 0.05$.

Instead of using coupled dissipative and random forces as thermostat in classical DPD, Lowe invented a new thermostat for use in coarse-grained simulations based on Andersen thermostat (called LA thermostat).[53] It is much effective on controlling the temperature and Galilean invariant. Correct fluid hydrodynamic behavior can be presented in this scheme, thus we adopt LA thermostat in our coarse-grained DPD simulations instead of using coupled dissipative and random forces. In LA thermostat, for each pair of interacting beads, we generate a relative velocity $\mathbf{v}_{ij}^o \cdot \hat{r}_{ij}$ from a Maxwell distribution $\xi_{ij}(2k_BT/m)^{1/2}$ with a probability $\Gamma\Delta t$, in which Γ is the collision frequency and ξ_{ij} is a Gaussian distributed random number. To conserve momentum, $\mathbf{v}_i = \mathbf{v}_i + \Delta_{ij}$, and $\mathbf{v}_j = \mathbf{v}_j - \Delta_{ij}$, where $2\Delta_{ij} = \hat{r}_{ij}(\mathbf{v}_{ij}^o - \mathbf{v}_{ij}) \cdot \hat{r}_{ij}$. In LA, the bath collision frequency Γ is related to the system viscosity.[53] Lowe found that the relation between viscosity η and Γ is $\eta \propto \Gamma$. Thus, by LA, we can easily tune up the viscosities of the components over several orders of magnitude to simulate different orders of diffusion dynamics.[38,54] To quickly approach to the relative diffusion equilibrium in our simulations, we choose $\Gamma = 10$ so that the coupling between diffusion and curing reaction process can be well manifested. The velocity Verlet algorithm is used to integrate the equations of motion.[55] Detailed integration scheme including LA thermostat can be found in refs 53, 54, and 56.

2.3. Defining Repulsive Parameters in DPD. There are several different ways to estimate interaction parameters in DPD simulations.[14,48,51] For example, in ref 48, the authors mapped the binding energies between different species at the atomistic level to define the DPD interaction parameters between polymer and clay. In another multiscale modeling approach, Scocchi et al.[14] proposed a similar route to determine the repulsive DPD parameters by mapping the energy values resulted from the atomistic MD simulations. In this research, we estimate the DPD interaction parameters between different components from Flory−Huggins χ-parameters, since Groot and Warren had established a well validated mapping scheme between them.[51]

Table 2. Atomistic MD Simulation Results for the Solubility Parameters of DDS, RA, and SA

	cell size (Å^3)	E_{coh} (kcal/mol)	δ ((cal/cm^3)$^{1/2}$)
DDS	$(22.89)^3$	22.43	10.29
RA	$(26.95)^3$	38.24	7.98
SA	$(27.89)^3$	149.72	7.33

To obtain the Flory−Huggins χ-parameters of the components at a specific temperature, we need to estimate their solubility parameters first by using atomistic MD simulations.[39,57] On the basis of the densities of the components at experimental temperature (423 K), canonical ensemble MD simulations are conducted for different components. The initial configurations with periodic boundary conditions are generated with the amorphous cell module in Materials Studio at 423 K with respective experimental densities. The COMPASS[45] force field is adopted in the simulations. The van der Waals interactions are based on cutoff treatment and the electrostatic interactions are dealt with standard Ewald summations.[47] We use a Berendsen thermostat[46] to control the target temperature. The integration time step is chosen as 1.0 fs, and the simulations last 1 ns, in which the last 200 ps trajectories are used for calculating ensemble averages. For the system containing k molecules of the same species, we can obtain the nonbonded energy of the model, E_{nb}^k. Then each molecule is extracted to vacuum to calculate the nonbonded energy for the individual molecule. Thus, the cohesive energy E_{coh} can be calculated via[57]

$$E_{coh} = \left(\sum_{i=1}^{k} E_{nb}^{\text{isolated}}(i) - E_{nb}^k\right)/k \quad (1)$$

where $E_{nb}^{\text{isolated}}(i)$ is the nonbonded energy for the ith isolated molecule in vacuum. The cohesive energy densities of the components at the experimental temperature, e_{coh}, can therefore be calculated, i.e., $e_{coh} = E_{coh}/V_m$, where V_m is the molar volume of the component. Subsequently, the solubility parameters of the components can be estimated with $\delta = (e_{coh})^{1/2}$. The simulation results are as shown in Table 2.

The Flory−Huggins interaction parameters χ at 423 K can therefore be calculated via[39,58,59]

$$\chi_{ij} = \frac{(\delta_i - \delta_j)^2 v_{\text{ref}}}{k_B T} \quad (2)$$

where δ_i and δ_j are the solubility parameters for component i and j, respectively, and v_{ref} is the reference bead volume. The reference bead volume v_{ref} can be taken as the average size of the coarse-grained beads, which is $\overline{v} = 409.42$ Å^3 in this study. Therefore, the values of χ_{ij} between different components are obtained.

Table 3. DPD Interaction Parameters between Different Components

α_{ij}	DDS	RA	SA
DDS	25.00	30.47	33.99
RA		25.00	25.43
SA			25.00

The empirical relation between Flory−Huggins χ parameters and DPD interaction parameters[51] is used to evaluate the DPD interaction parameters between different species:

$$\chi = (0.286 \pm 0.002)(\alpha_{ij} - \alpha_{ii}) \quad (\rho = 3) \tag{3}$$

where α_{ii}(=25) and α_{ij} are the DPD interaction parameters between the same and different types of species, respectively. The calculated DPD interaction parameters between different components, α_{ij}, are shown in Table 3. Obviously, the compatibility between the three components is high. Thus, we can expect an apparent mixing between them due to mutual diffusion.

2.4. Modeling Curing Reaction. We employ the idea in our previous works[40−42] by introducing the reaction probability P_r to model the curing reactions in DPD. In each reaction time interval $\tau = N_{step}\Delta t$ (where N_{step} is a constant number), if an active end meets several reactable beads (e.g., a bead containing the active amine hydrogen meets the beads containing epoxy groups or vice versa) in the reaction radius (taken the same as the interaction radius for convenience), first it randomly chooses one of the reactable beads as the reacting object. Subsequently, another random number is generated, and by checking if it is smaller than the preset P_r, we decide whether the reacting object will be connected to the active end or not. The model corresponds to the reaction process with a constant reaction rate. In the literatures, similar Monte Carlo-like reaction strategies were proposed to reflect the active energy barriers in chemical reactions.[60,61] In this study, the reaction probability P_r is similarly dependent on the activation energy barrier of the reaction, thus we assume that different reaction probabilities correspond to different reaction rates of the systems determined by different levels of reaction activation energies.[40] In the simulations, we adopt reaction probability P_r = 0.001 and the reaction time interval $\tau = N_{step}\Delta t = 1$ (i.e., the reaction may take place for once determined by P_r within a DPD time unit),[42] which represent a relatively moderate reaction with regard to the simulation time unit according to our previous experiences.

Here we follow the experimental treatment of this complex system to set up our simulations. First in DPD simulations, the reaction is switched off until a relative diffusion equilibrium, defined by the time that the front of spreading DDS beads arrives in the region very near to the surface, is reached. This step is mimicking the thermal mixing stage in experiments to relieve the interfacial tensions. Subsequently, the curing reaction is allowed to take place in the simulations until the conversion of the functional groups achieves over 80%. Finally the network structures can be obtained.

During the modeling of curing reactions, some important issues should be noted: (i) According to the experimental results,[1] we assume that the etherification reactions between the generated hydroxyl groups due to ring open and other epoxy groups can be neglected, as the same handling in ref 11. (ii) The terminal beads of RA and SA chains contain the epoxy groups; thus, these beads are considered as the active beads. During the curing reaction, at most one new bond can be formed from each of these beads, which corresponds to the reaction between the epoxy group with one amine group in DDS. (iii) For each DDS bead, at most four new bonds can be formed since one DDS molecule contains four reactive hydrogen atoms in two terminal amine groups. It should be noted, in CG level, the formation of the former two bonds from DDS bead can be considered as the consumption of two hydrogen atoms in primary amines (i.e., the primary curing reaction), while the latter two bonds are related to the secondary curing reaction. According to the experimental results of these reactions,[1] the secondary curing reaction corresponds to a higher activation energy, thus the reaction probability in the secondary curing reaction is set as 1/10 of the former, i.e., P_r = 0.0001, to represent a more difficult reaction in our simulations.

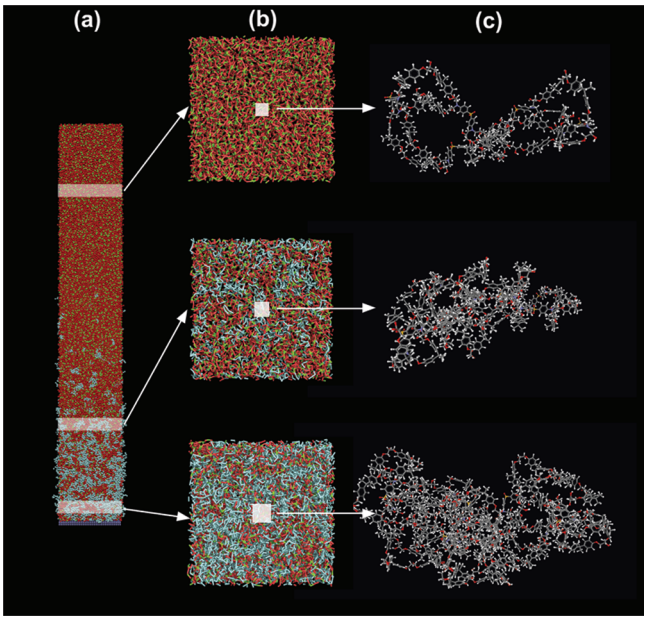

Figure 3. Network structures of the epoxy resin system with different resolutions of representation after the accomplishment of the curing reaction. In parts a and b with stick representations, the red stick represents the bond between RA bead and other beads, the green stick represents the bond between the curing agent DDS bead and other beads, while the cyan stick represents the bond between SA bead and other beads. Part c shows the reverse mapped all atomistic representation of the local network structures.

We then carry out simulations with curing reactions in this typical epoxy system. Figure 3 shows the network structures of the epoxy resin with different resolutions of representation after the accomplishment of the curing reactions. We can see a gradient change of the network composition due to the mutual diffusion between the components.

2.5. Reverse Mapping and All Atomistic MD Simulations. To analyze the mechanical properties of the epoxy resin after the curing reactions, we reverse-map the local CG structures into all atomistic structures based on the component and the cross-link distributions along z axis (i.e., the direction perpendicular to the surface). Actually, there are different ways to do reverse mapping from the results of a coarse-grained simulation. Since in the coarse-graining scheme, the correspondence between a coarse-grained bead with the underlying atomistic structures has been defined clearly, we therefore may insert the atoms into the space occupied by the coarse-grained beads to reconstruct the polymer

chains. We had used this reverse mapping procedure and rebuilt the polyethylene melt after coarse-grained simulations in previous studies.[38] However, it is not quite feasible to use this reverse mapping procedure on our epoxy systems in this research, because randomly generating bonds between atoms belonging to nearby coarse-grained beads will inevitably result in bond crossing through phenyl rings in the epoxy molecules. We then consider to use another reverse mapping scheme. As we know, in the coarse-grained simulations, the most important results are the component ratios and the cross-link density in a local network region. Therefore, we use these information to define our atomistic systems; i.e. in practice, we construct the atomistic systems with the same component ratios and cross-link density as those obtained from the CG simulations. The advantage of this reverse mapping scheme is that we can largely avoid the possibility of the bond penetrating into the phenyl rings. As a final step, after the reconstruction of the atomistic system, we also check all the phenyl rings to eliminate any bond penetrating by moving this bond out of the ring. The energetic unfavorable configuration will be easily relaxed in the following MD simulations.

To obtain the component ratios and the cross-link density in our CG model, we need to take into account all molecules with center of mass residing inside the selected reverse mapping region. For the network structure generated in our DPD simulations, we choose three representative locations along z axis to construct the all-atomistic network structures. In each location, first we construct an atomistic system with generally the same component ratios as that obtained from the CG system. Then the reactive groups in the molecules are bonded to construct the network structure with the cross-link density coinciding to the value obtained from CG simulations.

After the reverse mapping, to ensure that the atomistic structures are fully equilibrated for the calculation of T_g and mechanical properties, we use annealing algorithm via MD simulations to relax these structures. In the annealing algorithm, NVT simulations are performed at sequential temperatures from 250 to 600 K with an interval of 50K, then the temperature is decreased step by step to 250 K to finish one annealing loop. The final structures are then used in the following MD simulations to evaluate T_g and mechanical properties.

3. RESULTS AND DISCUSSION

The mesoscopic simulations are conducted in canonical ensemble with DPD method. The whole simulation is divided into two stages. The first stage is the diffusion stage, which is adopted to mimic the experimental relative diffusion equilibrium stage. In experiments, relative diffusion equilibrium means that component mutual diffusion without reaction will be kept until some DDS molecules arrive in the region near to the carbon fiber surface. After generating the initial configuration (as shown in Figure 2), DPD simulations without reactions are carried out to allow the components in the two layers to diffuse mutually due to their chemical potential diferences. The diffusion stage is accomplished when about 1% of the DDS beads diffuse into the layer 3 nm from the surface, representing the relative diffusion equilibrium in experiments. We find that 4.5×10^5 timesteps DPD simulations are enough in this stage for all the parallel samples. The second simulation stage is the curing reaction stage, in which, 1×10^6 timesteps DPD simulations are conducted with the curing reactions switched on to model the formation of network structures. In this stage, the functional group conversion higher than 80% will be achieved. As a result, the compositions at different network locations are quite different due to component mutual diffusion, as demonstrated in Figure 3a.

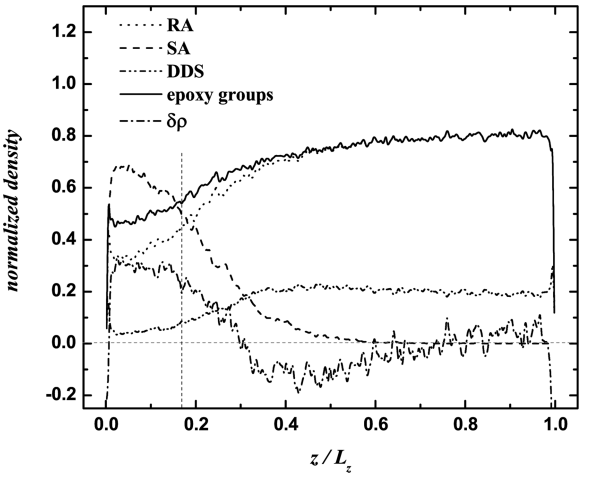

Figure 4. Gradient distribution in the z direction of the normalized density of different components after the accomplishment of the diffusion stage. Five independent samples are simulated under the same condition to calculate the mean value and the error bar. The error bars are not shown here for clarity.

We obtain the density distributions of different components along the direction perpendicular to the surface after the first stage of DPD simulations, as shown in Figure 4. The vertical dashed line in Figure 4 indicates the initial interface between DDS/RA and SA phases. The SA layer is on the left side, while the DDS/RA layer is on the right side of the vertical dashed line. The position at $z/L_z = 0$ means the location of the carbon fiber surface. We find that in SA dominating layer, RA has a higher normalized density than that of DDS along the z direction. It can be attributed to that, when some DDS beads diffuse near to the surface at relative diffusion equilibrium, a great amount of RA beads have reached there due to relatively better compatibility between RA and SA. As shown in Figure 4, SA does not diffuse deeply into the DDS/RA layer due to its low mobility. The distribution of epoxy groups with respect to that of amine groups should be an important factor to determine the local composition and the network structure. We also calculate the density distribution of total epoxy groups (as the sum of epoxy groups in RA and SA), as shown in Figure 4. We can find that the epoxy groups distribute uniformly in the DDS/RA layer, but show a slight decrease in the SA layer. This is mainly because that both SA and RA molecules possess two end epoxy groups, but SA molecules are much longer than RA. In comparison, DDS molecules (each DDS molecule possesses four amine groups) distribute uniformly in the DDS/RA layer, but show an obvious insufficiency in the SA layer. We define the difference between the two types of functional groups at each position perpendicular to the surface as $\delta\rho = \rho_{(epoxy)} - \rho_{(hydrogen)}$ The results are also shown in Figure 4, in which, the regions with $\delta\rho > 0$ indicate the insufficiency of amine hydrogen atoms in the curing reactions, while the regions with $\delta\rho < 0$ indicate the insufficiency of epoxy groups during the curing reactions. It is clear that in the region $z/L_z \leq 0.3$, the amine hydrogens are extremely insufficient, while in the region $0.3 \leq z/L_z \leq 0.7$ the epoxy groups become insufficient. In the region $z/L_z > 0.7$, the two types of functional groups are equivalent in molar ratio because they are mixed well in the

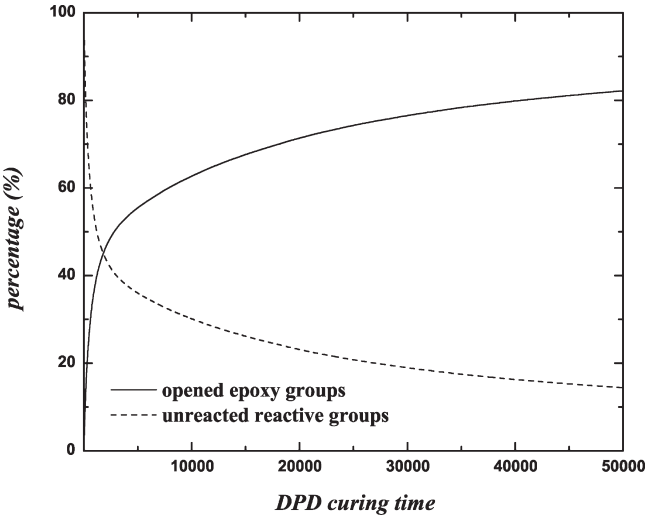

Figure 5. Time evolution of the conversion during the curing reaction. Five independent samples are simulated under the same condition to calculate the mean value and the error bar. The error bars are not shown here for clarity.

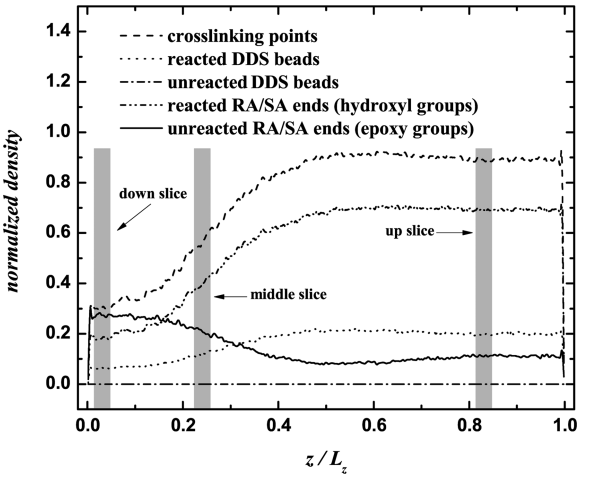

Figure 6. Gradient distribution in the z direction of the normalized density of different groups after the accomplishment of the reaction stage. Note that, the reacted DDS bead represents the DDS with at least one secondary or ternary amine group, while the unreacted DDS bead means that the two amine groups in the DDS are both primary ones. Five independent samples are simulated under the same condition to calculate the mean value and the error bar. The error bars are not shown here for clarity. The tagged gray regions indicate the selected up-, middle-, and down-slices for use in reverse mapping procedure.

beginning. As a result, we can expect a lack of cross-linking points in the region near to the surface, while a relatively higher cross-linking density in the top part of DDS/RA layer.

We switch on the curing reactions in the second stage of DPD simulation, then the epoxy groups consume the reactive amine hydrogens to gradually form the network structure. The extent of the curing reaction can be indicated by the percentage of opened epoxy groups (i.e., those attend the curing reactions) in the total original epoxy groups. The results are shown in Figure 5. In the early stage of the curing reactions (about 6×10^4 timesteps), the percentage of the opened epoxy groups increases sharply to a value about 50%, after that, the percentage increases quite slow. This result could be partially ascribed to our reaction model, in which both primary and secondary curing reactions are considered to reflect the experimental fact. The first two reactions of the DDS bead correspond to the transformations from primary to secondary amines (i.e., the primary curing reaction), while the other two reactions correspond to the transformations from secondary to ternary amines (i.e., the secondary curing reaction). The reaction probability of the secondary curing reaction is much smaller than that of the primary curing reaction. Therefore, the conversion of 50% epoxy groups generally corresponds to the consumption of the primary amines in the system, which is a very fast process. In the following 9.4×10^5 timesteps, the curing reaction is quite slow and the percentage of opened epoxy groups reaches over 80% finally. Besides the reason that the secondary curing reaction is slow in our model, another reason could be the diffusion slowing down in the late stage of curing reaction. As the curing reaction proceeds, the reactants become insufficient in local regions. Further curing reaction requires that the chemically active groups move around to find their reacting targets in the system. However, in the late stage of curing reactions, most of the components become part of the large network structure, thus the mobilities of the reactive beads are largely reduced and the curing reactions are effectively slowed down. We also use the percentage of unreacted reactive groups in the total original reactive groups to characterize the curing conversion, as shown by the dashed line in Figure 5. This value decreases sharply in the beginning of the curing reaction and then the decrease slows down apparently. We find that at last less than 20% of the reactive groups are still unreacted in the system. It should be noted that, at the end of the curing reaction, the sum of the value in the solid line and that in the dashed line is generally 100%, indicating that the 20% unreacted reactive groups are all epoxy groups. It implies that in the end of our simulations, there is nearly no primary amine (i.e., no unreacted DDS), and 20% of the secondary amines are waiting to be saturated by the rest of epoxy groups.

We further investigate the density distributions of the components and the reactive groups after the curing reactions in our simulations. The results are shown in Figure 6. It is clear that the density distribution of the unreacted DDS beads (including two primary amine groups) is basically zero, while in comparison, the reacted DDS beads (including at least one secondary or ternary amine group) distribute everywhere in the system. This indicates the extent of the curing reactions in our simulations, and supplies a possible way to directly compare to experimental results of the extent of curing reactions. Moreover, the density of the reacted RA/SA beads (i.e., the generated hydroxyl groups) is higher in the DDS/RA layer than that in the SA layer. It is mainly attributed to that the distribution of DDS in the SA layer is quite low, whereas in DDS/RA layer, both DDS and RA beads mix well. In contrast, the distribution of the unreacted RA/SA beads looks opposite. We can find a few unreacted epoxy groups in the DDS/RA layer but a large number of them in the SA layer. It is quite difficult for the long SA chains to diffuse into the network structure where most of the unsaturated secondary amine groups locate. Therefore, in the end of our simulations, the unreacted epoxy groups mostly distribute in the SA layer, whereas the unsaturated secondary amine groups mostly distribute in the DDS/RA layer. These two types of reactants can not easily meet together due to the high cross-link density of the network structure, thus further conversion of the functional groups slows down in the late stage of curing reactions.

Table 4. Mechanical Properties of the Network Structures at Different Representative Positions[a]

sample	bulk modulus (GPa)	shear modulus (GPa)
net-up	2.271 ± 0.344	1.217 ± 0.244
net-middle	3.415 ± 1.038	0.804 ± 0.461
net-down	2.510 ± 2.305	0.527 ± 0.385

[a] Five independent parallel simulations for each structure are used to calculate the mean value and the standard error.

To further analyze the mechanical properties of the network structure, it is necessary to obtain the cross-link density distribution after the curing reactions. Also as shown in Figure 6, the density of the cross-linking points in the DDS/RA layer is higher than that in the SA layer. We then choose three slices of the local network structures along z axis (as shown in Figure 6) and reverse map them into the all atom representations as illustrated in Figure 3c. In the following, we name the representative network structures as net-up, net-middle, and net-down from up to down along z-axis, respectively. Since the cross-link densities are different in the network structures, we expect to find a general dependence of the mechanical properties on the cross-link density at different locations. In literatures, there are some applications of MD simulations on the prediction of mechanical properties of polymers.[16,18,62−64] Here, we also adopt the constant-strain minimization method[65] to calculate the mechanical properties of three parts of network structures. In this method, the mechanical properties are obtained from changes in the total energy of the systems subjected to deformation. The stiffness matrix is derived from the second derivative of potential energy (U) with respect to the strain (ε),[65]

$$C_{ij} = \frac{1}{V}\left(\frac{\partial U^2}{\partial \varepsilon_i \partial \varepsilon_j}\right) = \frac{\partial \sigma_i}{\partial \varepsilon_j} \tag{4}$$

where V is the volume, ε_i is the ith component of the strain tensor and σ_i is the ith component of the stress tensor. Thus, the stiffness matrix of isotropic amorphous materials can be simply determined by two Lamé constants (λ, μ) as follows:

$$C_{ij} = \begin{pmatrix} 2\mu+\lambda & \lambda & \lambda & 0 & 0 & 0 \\ \lambda & 2\mu+\lambda & \lambda & 0 & 0 & 0 \\ \lambda & \lambda & 2\mu+\lambda & 0 & 0 & 0 \\ 0 & 0 & 0 & \mu & 0 & 0 \\ 0 & 0 & 0 & 0 & \mu & 0 \\ 0 & 0 & 0 & 0 & 0 & \mu \end{pmatrix} \tag{5}$$

From this symmetrical matrix, it is easy to derive the values of the two Lamé constants. Therefore, we can further calculate the characteristic modulus as: the bulk modulus $K = \lambda + (2/3)\,\mu$ and the shear modulus $G = \mu$, respectively.

Five independent parallel simulations for each structure are carried out to calculate the mean value and the standard error. The results are shown in Table 4. It is clear that for the three network structures, as the cross-link density increases from down slice to up slice, the shear modulus increases remarkably. But there is no apparent dependence of the bulk modulus on the cross-link density. We find that the results of the moduli are generally in harmony with those of the polymer systems obtained from MD simulations.[11,17,18] According to the calculated bulk and shear moduli, we can estimate the Poisson's ratios[65] of each network structure. The Poisson's ratios for net-up/middle/down structures are 0.27−0.40. We think these values are reasonable as compared with common polymer systems, for example, the Poisson's ratio for cross-linked poly(vinyl alcohol) by 1,2-ethanediol with conversion of 90% was found to be around 0.35 from MD simulations.[17]

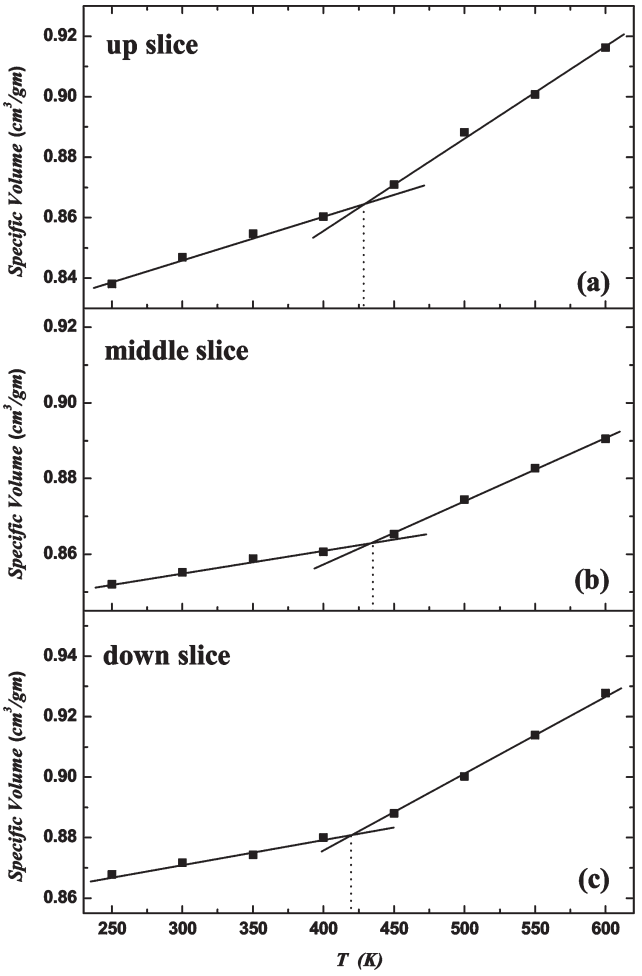

Figure 7. Relationship of specific volume and temperature for the three slices in the network: (a) the up slice; (b) the middle slice; (c) the down slice.

We also study the glass transition temperatures (T_g) of the three representative network structures via NPT ensemble all-atom MD simulations. The changes of specific volume with temperature are obtained in the MD simulations, by which we may estimate T_g from the slope change.[66,67] The temperature range between 250 and 600 K is scanned with the interval of 50 K. To make sure that the chain configurations are fully relaxed and the MD simulations are equilibrated, for each configuration the MD simulation is first performed for 250 ps at each target temperature. Then another simulation with 250 ps is performed to collect the data. As shown in Figure 7, we present the volume−temperature relations of the three network structures. From net-up to net-down, we find that the temperatures corresponding to the slope change in the volume−temperature plots of the three network structures are generally the same. It implies that the glass transition temperatures of the three network structures have no apparent differences. As we know, T_g correlates with the chain backbone flexibility. In general, the

more flexible the chain backbone is, the lower T_g will be. Backbone flexibility will be reduced due to cross-linking between chains, thus higher cross-link density normally corresponds to higher T_g. In the down slice of our samples, for the comparatively lower cross-link density, lower T_g is expected. However, the formation of highly cross-linked structures (even in the down slice) leads to a sharp reduction of the chain backbone flexibility in all the slice samples, which will eliminate the difference on the chain mobilities in different slices. Therefore, we find the T_g values of all the samples are close to each other. Thus, we may conclude that, the cross-link is too dense in this composite material, so that the cross-link density influence on T_g is small.

4. CONCLUSIONS

In this study, the influence of the interplay between diffusion and curing reaction on the mechanical properties of a typical epoxy resin system is investigated via multiscale simulations. On the basis of the multiscale simulation strategy, we construct the mesoscopic DPD model coupled with the curing reaction to simulate the mutual diffusion process between different components as well as the formation of network structure in the epoxy resin system. We then reverse map the coarse-grained structure back to the all atomistic representation, and analyze the mechanical properties as well as the thermal mechanical properties of different network structures. This multiscale simulation strategy is not limited to this specific system, but also applicable in other complex systems with competing dynamic influencing factors.

AUTHOR INFORMATION

Corresponding Author

*E-mail: (M.L.) leemy@buaa.edu.cn; (Z.-Y.L.) luzhy@jlu.edu.

ACKNOWLEDGMENT

This work is supported by National Science Foundation of China (21025416, 50803002, 50930001) and China Postdoctoral Science Foundation (20110491295).

REFERENCES

(1) Girard-Reydet, E.; Riccardi, C. C.; Sautereau, H.; Pascault, J. P. *Macromolecues* **1995**, *28*, 7599.
(2) Girard-Reydet, E.; Riccardi, C. C.; Sautereau, H.; Pascault, J. P. *Macromolecues* **1995**, *28*, 7608.
(3) Lahlali, D.; Naffakh, M.; Dumon, M. *Polym. Eng. Sci.* **2005**, *45*, 1581.
(4) Blancoa, M.; Corcuera, M. A.; Riccardi, C. C.; Mondragon, I. *Polymer* **2005**, *46*, 7989.
(5) Eloundou, J. P. *Eur. Polym. J.* **1999**, *35*, 1481.
(6) Tang, A. C.; Li, Z. S.; Sun, C. C.; Tang, X. Y. *Macromolecues* **1988**, *21*, 797.
(7) Xiao, X. C.; Li, Z. S.; Sun, C. C.; Tang, A. C. *Macromolecues* **1995**, *28*, 2738.
(8) Kuchanov, S.; Slot, H.; Stroeks, A. *Prog. Polym. Sci.* **2004**, *29*, 563.
(9) Yarovsky, I.; Evans, E. *Polymer* **2002**, *43*, 963.
(10) Gou, J. H.; Minaie, B.; Wang, B.; Liang, Z. Y.; Zhang, C. *Comput. Mater. Sci.* **2004**, *31*, 225.
(11) Wu, C. F.; Xu, W. J. *Polymer* **2006**, *47*, 6004.
(12) Wu, C.-F.; Xu, W.-J. *Polymer* **2007**, *48*, 5802.
(13) Lin, P.-H.; Khare, R. *Macromolecues* **2009**, *42*, 4319.
(14) Scocchi, G.; Posocco, P.; Fermeglia, M.; Pricl, S. *J. Phys. Chem. B* **2007**, *111*, 2143.
(15) Dömötör, G.; Hentschke, R. *Macromol. Thoery Simul.* **2004**, *13*, 506.
(16) Fan, H.-B.; Yuen, M. M. F. *Polymer* **2007**, *48*, 2174.
(17) Bermejo, J. S.; Ugarte, C. M. *Macromol. Thoery Simul.* **2009**, *18*, 317.
(18) Bermejo, J. S.; Ugarte, C. M. *Macromol. Thoery Simul.* **2009**, *18*, 259.
(19) Varshney, V.; Patnaik, S. S.; Roy, A. K.; Farmer, B. L. *Macromolecules* **2008**, *41*, 6837.
(20) Mijovie, J.; Zhang, H. *J. Phys. Chem. B* **2004**, *108*, 2557.
(21) Flory, P. J. *J. Am. Chem. Soc.* **1941**, *63*, 3083.
(22) Stockmayer, W. H. *J. Chem. Phys.* **1943**, *11*, 45.
(23) Gordon, M. *Proc. R. Soc. London, A* **1962**, *268*, 240.
(24) Miller, D. R.; Macosko, C. W. *Macromolecules* **1976**, *9*, 206.
(25) Shibayama, M. *Polymer J* **2011**, *43*, 18.
(26) Komarov, P. V.; Chiu, Y.-T.; Chen, S.-M.; Khalatur, P. G.; Reineker, P. *Macromolecules* **2007**, *40*, 8104.
(27) Duering, E. R.; Kremer, K.; Grest, G. S. *Phys. Rev. Lett.* **1991**, *67*, 3531.
(28) Sotta, P.; Higgs, P. G.; Depner, M.; Deloche, B. *Macromolecules* **1995**, *28*, 7208.
(29) Trautenberg, H.; Sommer, J.-U.; Göritz, D. *J. Chem. Soc., Faraday Trans.* **1995**, *91*, 2649.
(30) Escobedo, F. A.; de Pablo, J. J. *J. Chem. Phys.* **1996**, *104*, 4788.
(31) Kenkhare, N. R.; Smith, S. W.; Hall, C. K.; Khan, S. A. *Macromolecules* **1998**, *31*, 5861.
(32) Lu, Z.-Y.; Hentschke, R. *Phys. Rev. E* **2001**, *63*, 051801.
(33) Lu, Z.-Y.; Hentschke, R. *Phys. Rev. E* **2002**, *65*, 041807.
(34) Lu, Z.-Y.; Hentschke, R. *Phys. Rev. E* **2002**, *66*, 041803.
(35) Lu, Z.-Y.; Hentschke, R. *Phys. Rev. E* **2003**, *67*, 061807.
(36) Aydt, E. M.; Hentschke, R. *J. Chem. Phys.* **2005**, *112*, 5480.
(37) Hörstermann, H.; Hentschke, R.; Amkreutz, M.; Hoffmann, M.; Wirts-Rütters, M. *J. Phys. Chem. B* **2010**, *114*, 17013.
(38) Chen, L.-J.; Lu, Z.-Y.; Qian, H.-J.; Li, Z.-S.; Sun, C.-C. *J. Phys. Chem. B* **2006**, *110*, 24093.
(39) Zhao, Y.; You, L.-Y.; Lu, Z.-Y.; Sun, C.-C. *Polymer* **2009**, *50*, 5333.
(40) Liu, H.; Qian, H.-J.; Zhao, Y.; Lu, Z.-Y. *J. Chem. Phys.* **2007**, *127*, 144903.
(41) Liu, H.; Xue, Y.-H.; Qian, H.-J.; Lu, Z.-Y.; Sun, C.-C. *J. Chem. Phys.* **2008**, *129*, 024902.
(42) Liu, H.; Li, M.; Lu, Z.-Y.; Zhang, Z.-G.; Sun, C.-C. *Macromolecules* **2009**, *42*, 2863.
(43) Dai, Z.-S.; Zhang, B.-Y.; Shi, F.-H.; Li, M.; Zhang, Z.-G.; Gu, Y.-Z. *Appl. Surf. Sci.* **2011**, *257*, 8457.
(44) http://accelrys.com/products/materials-studio/
(45) Sun, H. *J. Phys. Chem. B* **1998**, *102*, 7338.
(46) Beredsen, H. J. C.; Postma, J. P. M.; van Gusteren, W. F.; DiNola, A.; Haak, J. R. *J. Chem. Phys.* **1984**, *81*, 3684.
(47) Ewald, P. P. *Ann. Phys. (Leipzig)* **1921**, *64*, 253.
(48) Toth, R.; Voorn, D.-J.; Handgraaf, J.-W.; Fraaije, J. G. E. M.; Fermeglia, M.; Pricl, S.; Posocco, P. *Macromolecules* **2009**, *42*, 8260.
(49) Xue, Y.-H.; Liu, H.; Lu, Z.-Y.; Liang, X.-Z. *J. Chem. Phys.* **2010**, *132*, 044903.
(50) Pivkin, I. V.; Karniadakis, G. E. *J. Comput. Phys.* **2005**, *207*, 114.
(51) Groot, R. D.; Warren, P. B. *J. Chem. Phys.* **1997**, *107*, 4423.
(52) Groot, R. D.; Madden, T. J. *J. Chem. Phys.* **1998**, *108*, 8713.
(53) Lowe, C. P. *Europhys. Lett.* **1999**, *47*, 145.
(54) Chen, L.-J.; Lu, Z.-Y.; Qian, H.-J.; Li, Z.-S.; Sun, C.-C. *J. Chem. Phys.* **2005**, *122*, 104907.
(55) Allen, M. P.; Tildesley, D. J. *Computer Simulation of Liquids*; Clarendon: Oxford, U.K., 1987.
(56) Vatullainen, I.; Kartunnen, M.; Besold, G.; Polson, J. M. *J. Chem. Phys.* **2002**, *116*, 3967.
(57) Li, Z.-W.; Lu, Z.-Y.; Sun, Z.-Y.; Li, Z.-S.; An, L.-J. *J. Phys. Chem. B* **2007**, *111*, 5934.
(58) Fermeglia, M.; Cosoli, P.; Ferrone, M.; Piccarolo, S.; Mensitieri, G.; Pricl, S. *Polymer* **2006**, *47*, 5979.

(59) Fan, Z. J.; Williams, M. C.; Choi, P. *Polymer* **2002**, *43*, 1497.
(60) Hoy, R. S.; Fredrickson, G. H. *J. Chem. Phys.* **2009**, *131*, 224902.
(61) Meng, L.-Y.; Shang, Y.; Li, Q.-K.; Li, Y.-F.; Zhan, X.-W.; Shuai, Z.-G.; Kimber, R. G. E.; Walker, A. B. *J. Phys. Chem. B* **2010**, *114*, 36.
(62) Soto-Figueroa, C.; Rodríguez-Hidalgo, M.-R.; Martínez-Magadán, J.-M. *Polymer* **2005**, *46*, 7485.
(63) Seung, S. J.; Won, H. J. *Macromol. Theory Simul.* **1999**, *8*, 1.
(64) Pedone, A.; Malavasi, G.; Cormack, A. N.; Segre, U.; Menziani, M. C. *Theor. Chem. Acc.* **2008**, *120*, 557.
(65) Theodorou, D. N.; Suter, U. W. *Macromolecules* **1986**, *19*, 139.
(66) Han, J. C.; Gee, R. H.; Boyd, R. H. *Macromolecules* **1994**, *27*, 7781.
(67) Bharadwaj, R. K.; Berry, R. J.; Farmer, B. L. *Polymer* **2000**, *41*, 7209.